2D porous Fe_2O_3/graphitic-C_3N_4/graphene ternary nanocomposite with multifunctions of catalytic hydrogenation, chromium(VI) adsorption and detoxification

Yu-Ting Zhuang, Ting-Ting Zhu, Man Ruan, Yong-Liang Yu* and Jian-Hua Wang*

Research Center for Analytical Sciences, College of Sciences, Northeastern University, Box 332, Shenyang 110819, China

*Corresponding author.

E-mail: yuyl@mail.neu.edu.cn (Y.-L. Yu), jianhuajrz@mail.neu.edu.cn (J.-H. Wang).

Tel: +86 24 83688944; Fax: +86 24 83676698

Electronic Supplementary Information

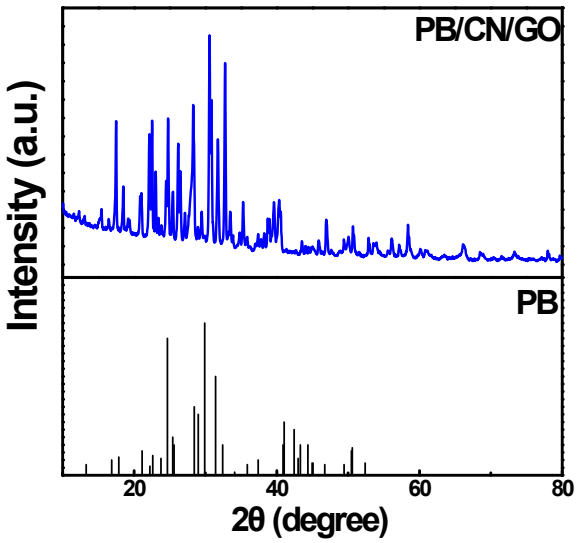

Fig. S1 XRD pattern of PB/urea/GO and Joint Committee on Powder Diffraction Standards (JCPDS) card for PB.

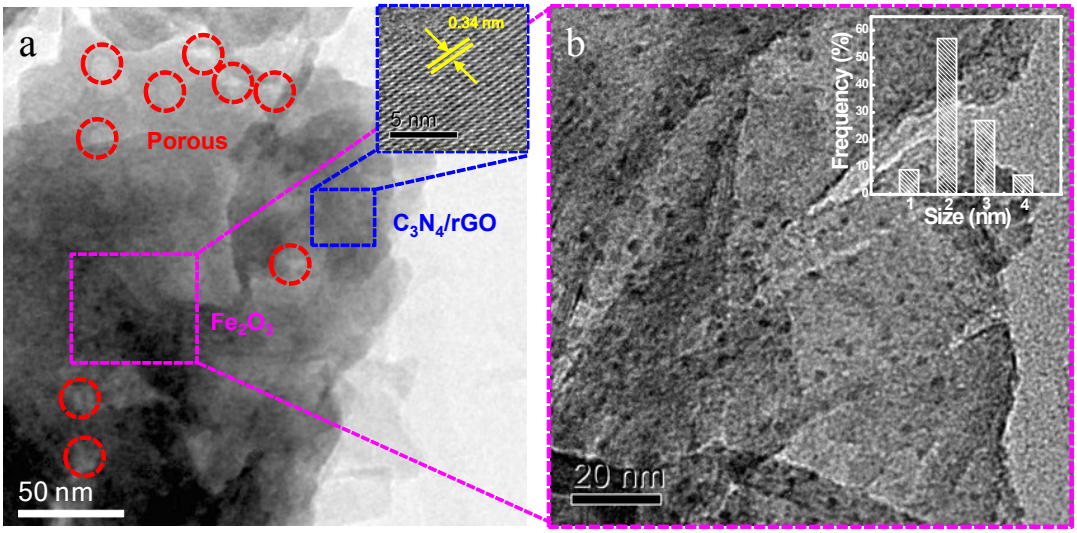

Fig. S2 (a) TEM image of FeCNG-127, inset: HRTEM image of FeCNG-127 from the area labelled by the rectangular frame in (a); (b) HRTEM image of FeCNG-127 from the area labelled by the rectangular frame in (a), inset: particle size distribution of Fe_2O_3 particles in FeCNG-127.

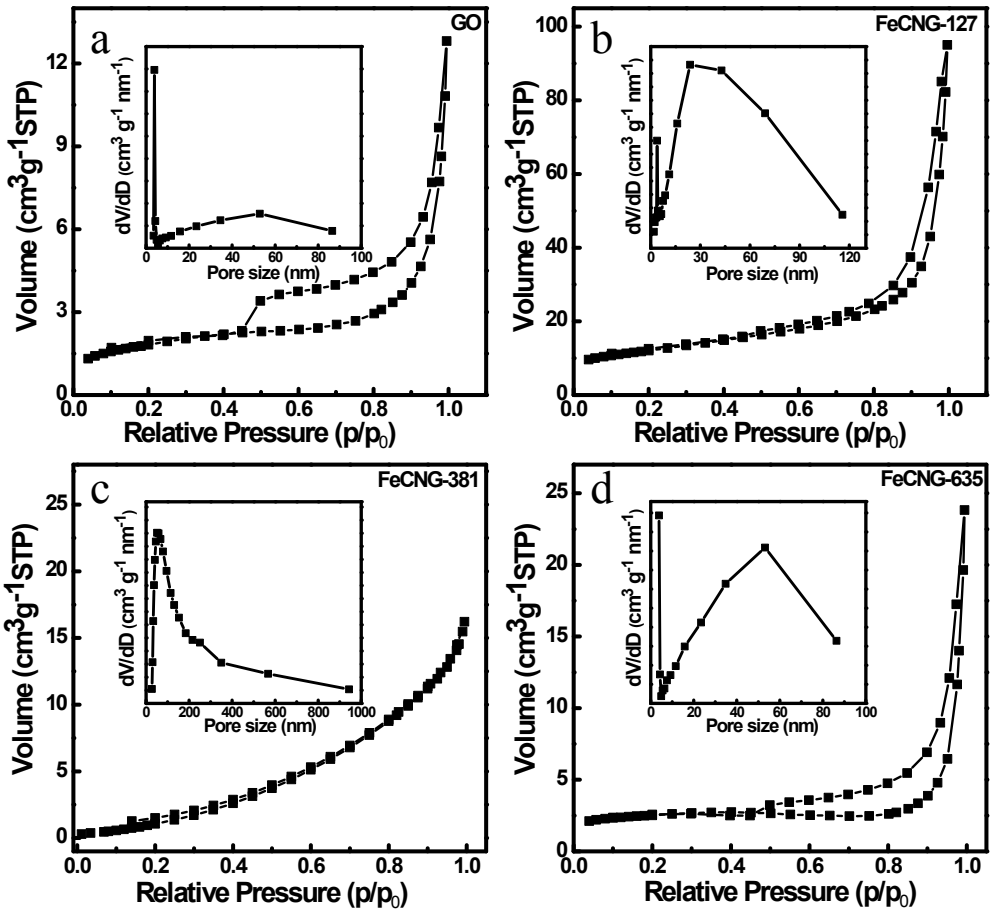

Fig. S3 Nitrogen adsorption/desorption isotherms and pore size distributions of (a) GO, (b) FeCNG-127, (c) FeCNG-381 and (d) FeCNG-635.

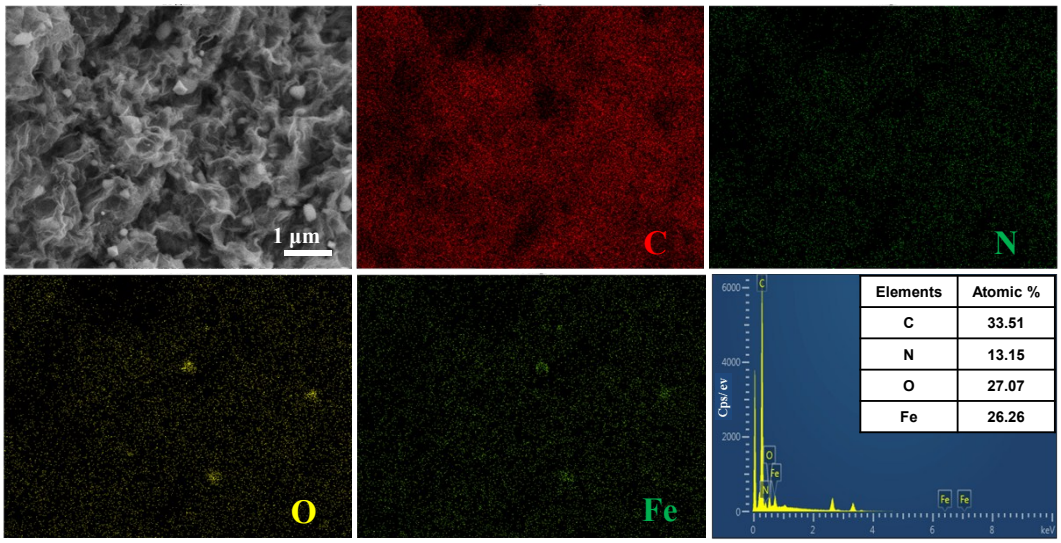

Fig. S4 Element mapping images and EDS analysis of FeCNG-127.

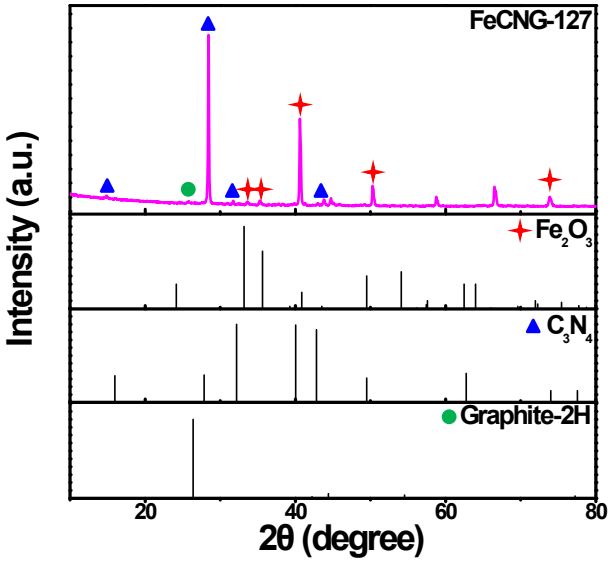

Fig. S5 XRD patterns of FeCNG-127 and JCPDS cards for Fe_2O_3, C_3N_4 and Graphite-2H.

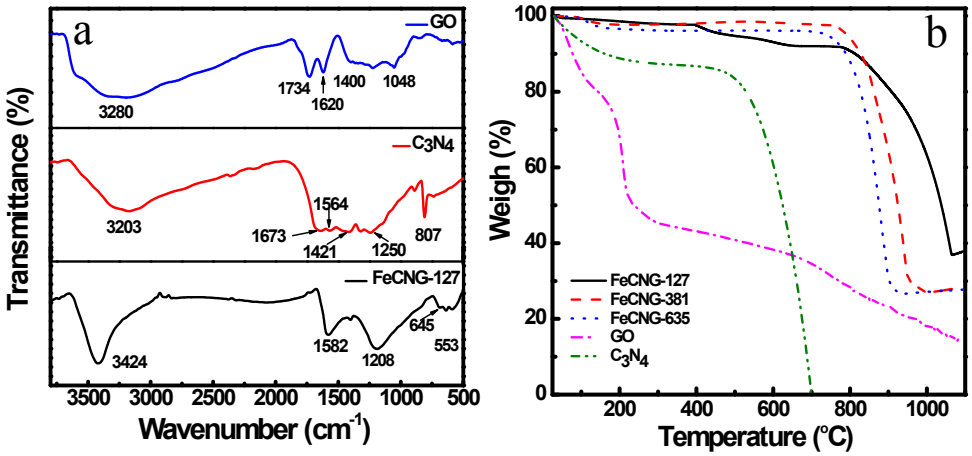

Fig. S6 (a) FT-IR spectra of GO, C_3N_4 and FeCNG-127; (b) TGA curves of GO, C_3N_4, FeCNG-127, FeCNG-381 and FeCNG-635 in N_2 atmosphere.

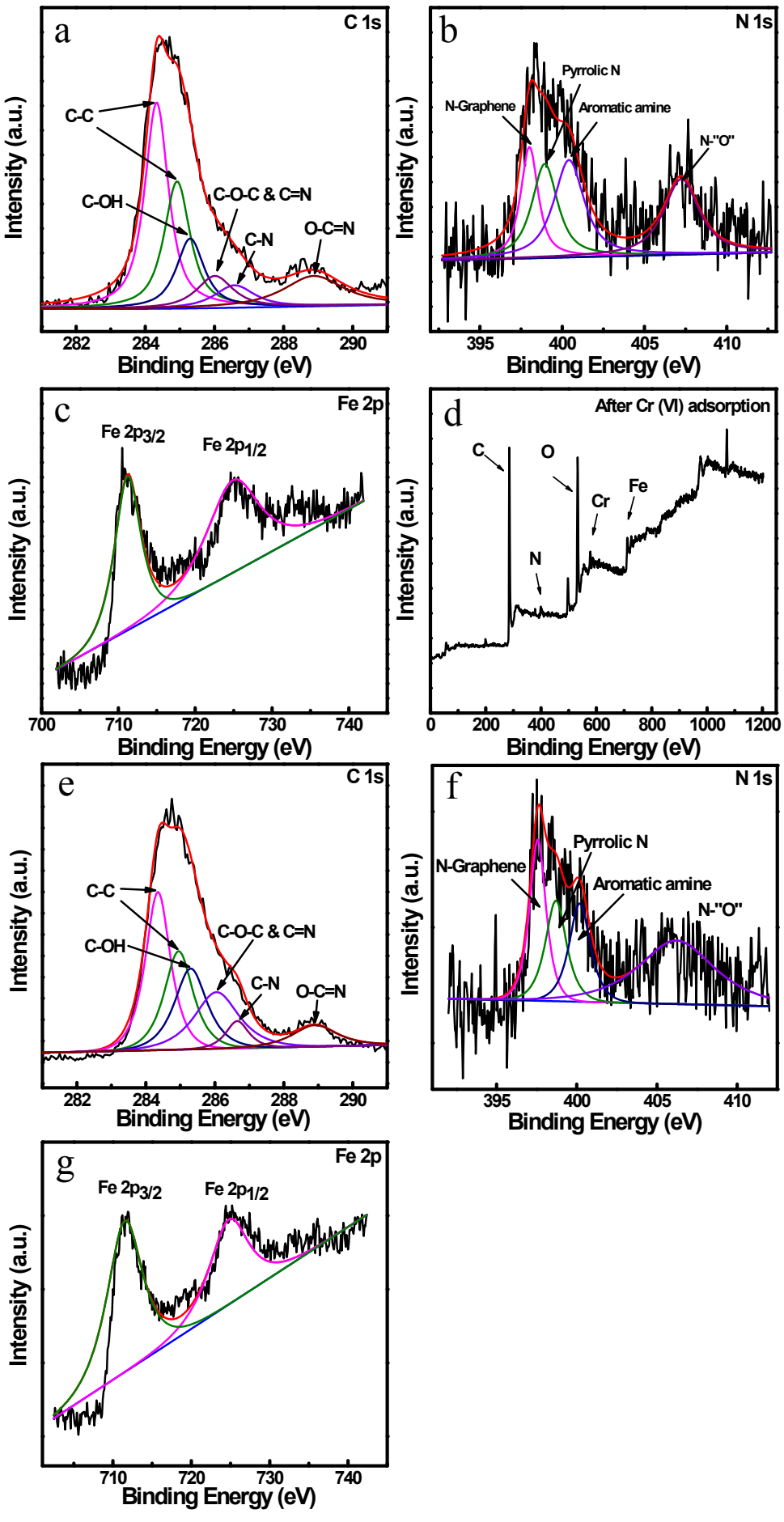
a
C 1s
C-C
C-OH
C-O-C & C=N
C-N
O-C=N
Intensity (a.u.)
282
284
286
288
290
Binding Energy (eV)
b
N 1s
Pyrrolic N
N-Graphene
Aromatic amine
N-"O"
Intensity (a.u.)
395
400
405
410
Binding Energy (eV)
c
Fe 2p
Fe 2p3/2
Fe 2p1/2
Intensity (a.u.)
700
710
720
730
740
Binding Energy (eV)
d
After Cr (VI) adsorption
C
O
Cr
Fe
N
Intensity (a.u.)
0
200
400
600
800
1000
1200
Binding Energy (eV)
e
C 1s
C-C
C-OH
C-O-C & C=N
C-N
O-C=N
Intensity (a.u.)
282
284
286
288
290
Binding Energy (eV)
f
N 1s
Pyrrolic N
N-Graphene
Aromatic amine
N-"O"
Intensity (a.u.)
395
400
405
410
Binding Energy (eV)
g
Fe 2p
Fe 2p3/2
Fe 2p1/2
Intensity (a.u.)
710
720
730
740
Binding Energy (eV)

Fig. S7 (a) C 1s spectrum of FeCNG-127 before Cr(VI) adsorption; (b) N 1s spectrum of FeCNG-127 before Cr(VI) adsorption; (c) Fe 2p spectrum of FeCNG-127 before Cr(VI) adsorption; (d) XPS survey spectrum of FeCNG-127 after Cr(VI) adsorption; (e) C 1s spectrum of FeCNG-127 after Cr(VI) adsorption; (f) N 1s spectrum of FeCNG-127 after Cr(VI) adsorption; (g) Fe 2p spectrum of FeCNG-127 after Cr(VI) adsorption.

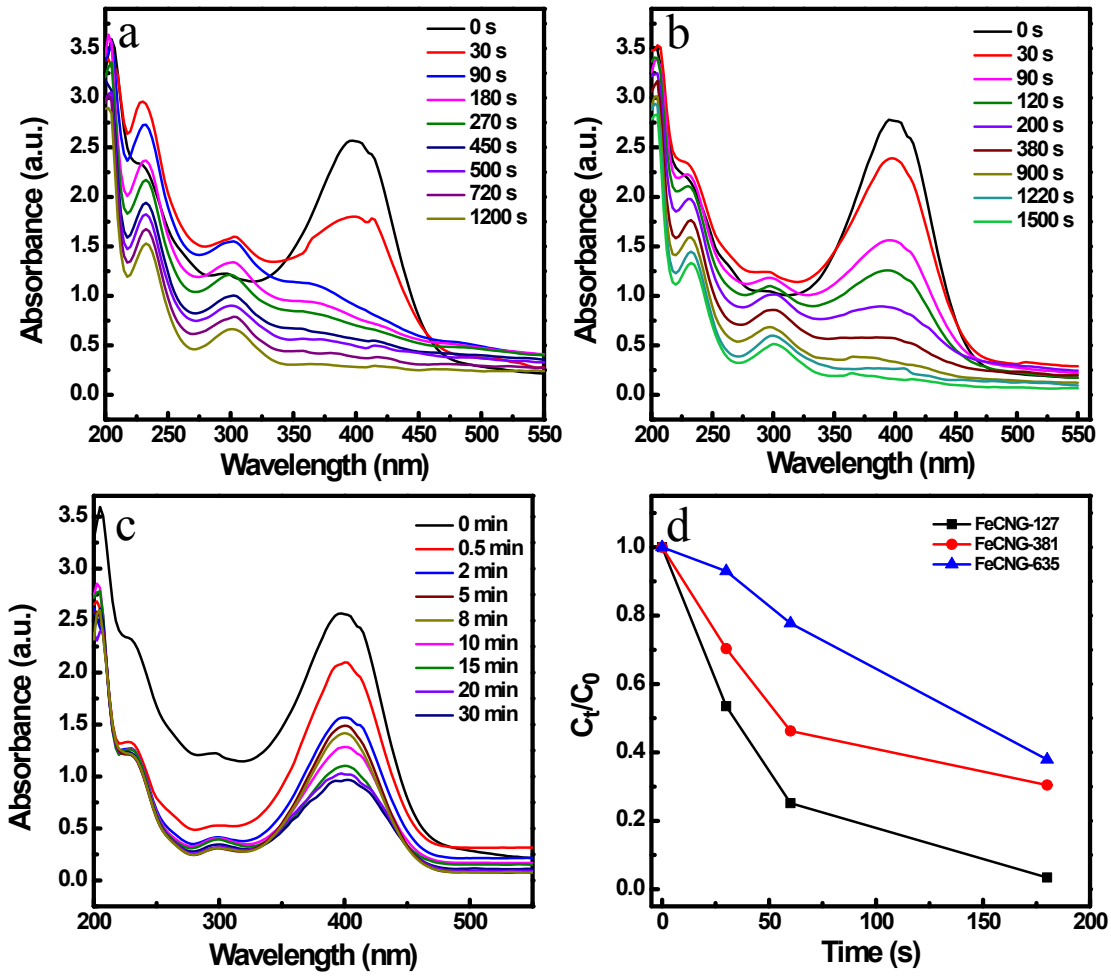

Fig. S8 (a) Time-dependent absorption spectra for the catalytic reduction of 4-NP by $NaBH_4$ in the presence of 1 mg of different catalysts: (a) FeCNG-381, (b) FeCNG-635 and (c) rGO-127; (d) Adsorption rate of the catalytic reduction of 4-NP by $NaBH_4$ in the presence of 1 mg of different catalysts. Conditions: 4-NP: 0.005M; $NaBH_4$: 0.02M; 25°C.

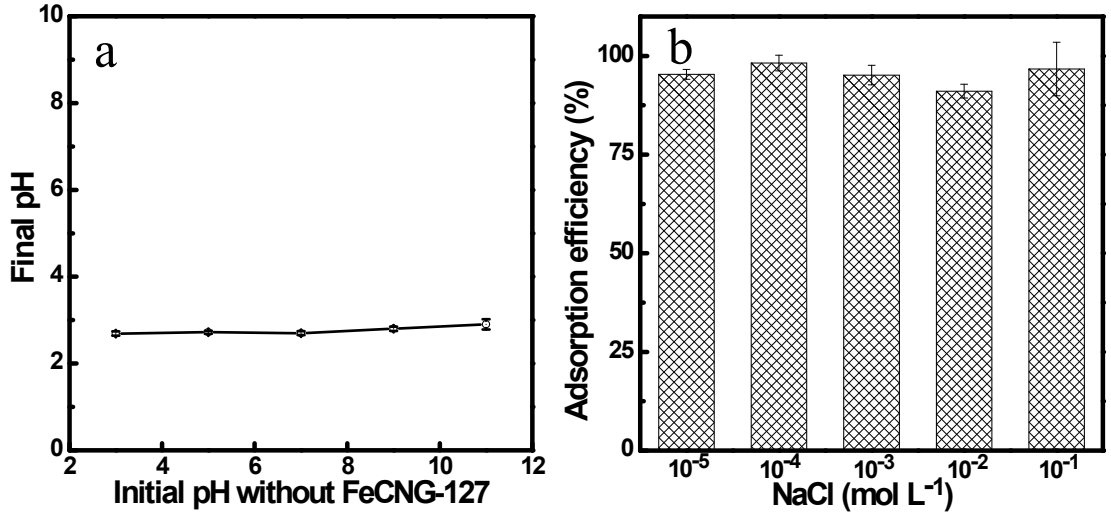

Fig. S9 (a) Variation of the final pH after immersion of FeCNG-127 into aqueous solutions with different pH values; (b) Effect of NaCl on the adsorption of Cr(VI) by FeCNG-127. Conditions: adsorbent dosage: 0.5 g L^{-1}; Cr(VI) concentration: 5 mg L^{-1}; shaking speed: 70 rpm; contact time: 6 h.

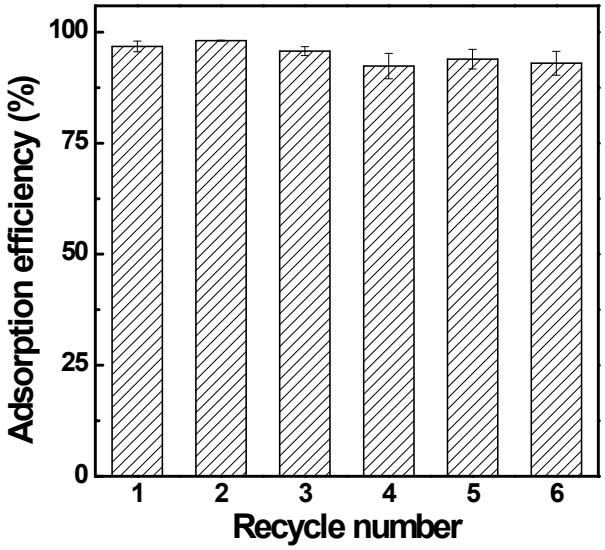

Fig. S10 Effect of recycling number on the adsorption of Cr(VI) by FeCNG-127. Conditions: adsorbent dosage: 0.5 g L^{-1}; Cr(VI) concentration: 5 mg L^{-1}; shaking speed: 70 rpm; contact time: 6 h.

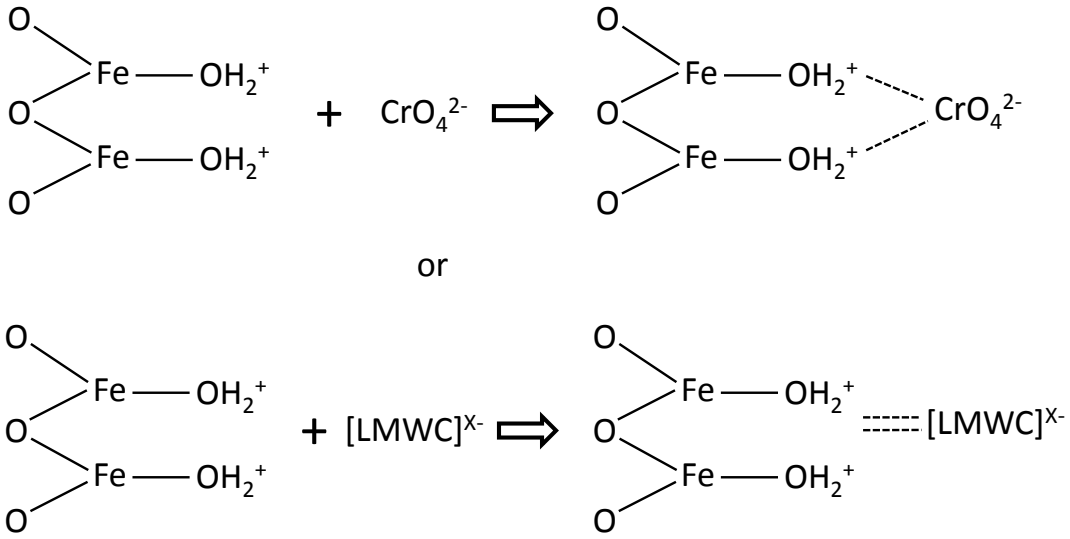

Scheme S1 Speculated mechanisms for the adsorption of Cr(VI) by FeCNG.

Table S1 Comparison of catalytic performance of recently reported catalysts towards *p*-nitrophenol reduction.

Catalyst	Dosage (mg)	k (min^{-1})	Ref.
$Co_{0.85}Se$-Fe_3O_4 nanocomposite	1	0.393	[1]
Ni/graphene nanostructure	3	0.702	[2]
Nickel/nanoporous carbon composite	0.3	0.168	[3]
$NiCo_2$ alloy	1	0.0735	[4]
Alloyed Cu/Ag bimetallic nanoparticles	2	0.237	[5]
Au-Fe_3O_4 hybrid nanoparticles	1	0.629	[6]
FeCNG-127	1	1.11	This work

Table S2 Adsorption kinetics fitting results for Cr(VI) adsorption on FeCNG-127 by pseudo-first-order and pseudo-second-order.

Pseudo-first-order model			Pseudo-second-order model		
Q_e (mg g^{-1})	k_1 (min^{-1})	R^2	Q_e (mg g^{-1})	k_2 [g (mg min)$^{-1}$]	R^2
3.03	0.00516	0.8548	10.2	0.00926	0.9993

References

1 J. M. Song, S. S. Zhang and S. H. Yu, *Small*, 2014, **10**, 717-724.

2 Y. G. Wu, M. Wen, Q. S. Wu and H. Fang, *J. Phys. Chem. C*, 2014, **118**, 6307-6313.

3 Y. Yang, Y. Zhang, C. J. Sun, X. Li, W. Zhang, X. Ma, Y. Ren and X. Zhang, *ChemCatChem*, 2014, **6**, 3084-3090.

4 K. L. Wu, X. W. Wei, X. M. Zhou, D. H. Wu, X. W. Liu, Y. Ye and Q. Wang, *J. Phys. Chem. C*, 2011, **115**, 16268-16274.

5 W. Wu, M. Lei, S. Yang, L. Zhou, L. Liu, X. Xiao, C. Jiang and V. A. L. Roy, *J. Mater. Chem. A*, 2015, **3**, 3450-3455.

6 X. W. Meng, B. Li, X. L. Ren, L. F. Tan, Z. B. Huang and F. Q. Tang, *J. Mater. Chem. A*, 2013, **1**, 10513-10517.